Available online at www.sciencedirect.com
ScienceDirect
ELSEVIER
Nuclear Instruments and Methods in Physics Research A 578 (2007) 47–54
NUCLEAR INSTRUMENTS & METHODS IN PHYSICS RESEARCH Section A
www.elsevier.com/locate/nima

Tomography reconstruction of the intensity distribution in a beam cross-section using optical diagnostics

G.E. Belyaev[a], I.V. Roudskoy[a,*], D. Gardès[b], P. Aussetn[b], A. Olivier[b]

[a]*ITEP, Moscow, Russia*
[b]*IPN, 91406 Orsay, France*

Received 29 March 2007; accepted 12 May 2007
Available online 24 May 2007

Abstract

An original experiment on tomography reconstruction of the intensity distribution in a beam cross-section was performed. It is based on an optical mapping of the beam scintillation due to interaction with the residual gas. Dedicated software realizing the algebraic reconstruction techniques was developed. In accordance with numerical simulations and experimental results, 4–8 projections are sufficient in most of the cases to reconstitute the intensity distribution in the cross-section with a good accuracy.

PACS: 29.27.Fh; 42.30.Wb

Keywords: Beam diagnostics; Optical diagnostics; Tomographic reconstruction

1. Introduction

The classical ways to measure the ion current density distribution in any ion beam cross-section are interceptive. They can no longer be used when the beam intensity (or the energy of ions) increases at such a point that they start to be damaged. All other weakly or non-interceptive diagnostic tools that are widely used such as wire scanners, ionization profile monitors or optical beam profilers collect a signal along the entire line-of-sight producing a projection of the beam intensity distribution. Therefore, some reconstruction methods are required to recover the original two-dimensional (2D) density distribution from the experimental data. In the simplest case of axisymmetry, the well-known Abel inversion may be applied to do that. But as soon as the measured projection becomes asymmetrical, the problem becomes more complicated. The only way to solve it is to increase the number of measured projections and to use a tomographic technique for a proper reconstruction.

Even if the projections may be deduced from any of the above-mentioned method, as far as the practical realization of the tomographic reconstruction is concerned, an optical diagnostics of ion beam looks attractive. Mapping the residual gas scintillation induced by the projectile beam ions with a CCD camera appears as one of the most suitable techniques. In spite of some inherent drawbacks, the optical diagnostics is the only easy way to get the necessary number of projections at different view angles and simultaneously. It is efficient in a very wide range of beam intensities in both continuous and pulsed modes. Combined with a monochromator, this diagnostics enables not only to distinguish the light emission from the residual gas and the accelerated ions, but also to separate the different components (both in the mass and in the charge state) of ions in the beams of mixed structure [1]. Moreover, with an appropriate optical arrangement, only one CCD camera would be needed to collect and record all the projections. This work presents the first step to demonstrate practically the merits of the optical tomography of ion beams.

2. Algebraic reconstruction technique

To not confuse the terms hereinafter, we shall use the term "beam cross-section" for 2D distribution of beam current

*Corresponding author. Tel.: +7 495 1299689; fax: +7 495 1233028.
E-mail address: Igor.Roudskoy@itep.ru (I.V. Roudskoy).

0168-9002/$ - see front matter © 2007 Elsevier B.V. All rights reserved.
doi:10.1016/j.nima.2007.05.205

density $j(x,y)$ in a certain cross-section of the beam. The value of the beam current density $J(x) = j(x,y_0)$ at a fixed y_0 will be referred as a "beam profile" and the integral over some direction (defined by angle α) of the distribution will be referred as a "projection" of the cross-section in this direction

$$g_\alpha(\rho) = \int_{l(\alpha,\rho)} j(x,y)\,\mathrm{d}l.$$

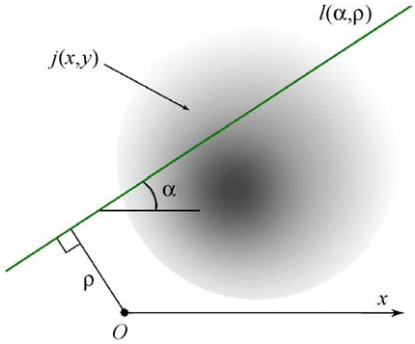

Fig. 1. Building up an image projection from the original 2D distribution. (The axis of the ordinates is not plotted here for purposes of clarity.)

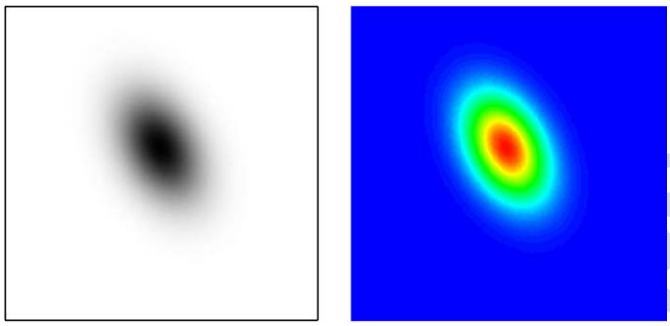

Fig. 2. Depicting of an input image (on the left) to multicolor scale.

Here, ρ is the distance of a line-of-sight $l(\alpha,\rho)$ from any set point of origin O as depicted in Fig. 1.

This integral is what optical and other non-interceptive diagnostics listed above are able to measure. The purpose of any beam diagnostics is to reconstitute the original 2D distribution of the current density $j(x,y)$ using a set of available projections $g_\alpha(\rho)$.

This problem belongs to the class of ill-defined or ill-conditioned inverse problems. Since 1917, when the problem was recognized and solved for the first time by Radon [2], few effective indirect algorithms of reconstruction have been developed. One of them, proving a good efficiency when the number of projections is small, is the algebraic reconstruction technique (ART) [3]. It is a very plain technique consisting in back projecting of available projections onto the reconstructed region. It exploits the fact that, having no a priori knowledge about the original 2D distribution, we can only suppose that the value of each point $g_\alpha(\rho_i)$ in a projection is uniformly distributed along the correspondent line in the reconstructed picture. Carrying out the procedure with each point of each projection we create a first approximation $j^{(1)}(x,y)$. This approximation is projected down again and each new projection $g_\alpha^{(1)}(\rho)$ of the approximation is compared with the original one $g_\alpha(\rho)$. The difference between them $(g_\alpha^{(1)}(\rho) - g_\alpha(\rho))$ is back-projected again. This yields an improved approximation $j^{(2)}(x,y)$ and so forth. The iteration continues while the approximation is improved. In other words, while $\varepsilon_{i+1} < \varepsilon_i$, where

$$\varepsilon_i = \sqrt{\sum_{\rho,\alpha} \left(g_\alpha^{(i)}(\rho) - g_\alpha(\rho)\right)^2}$$

is the total discrepancy between the original projections and projections obtained at ith iteration step.

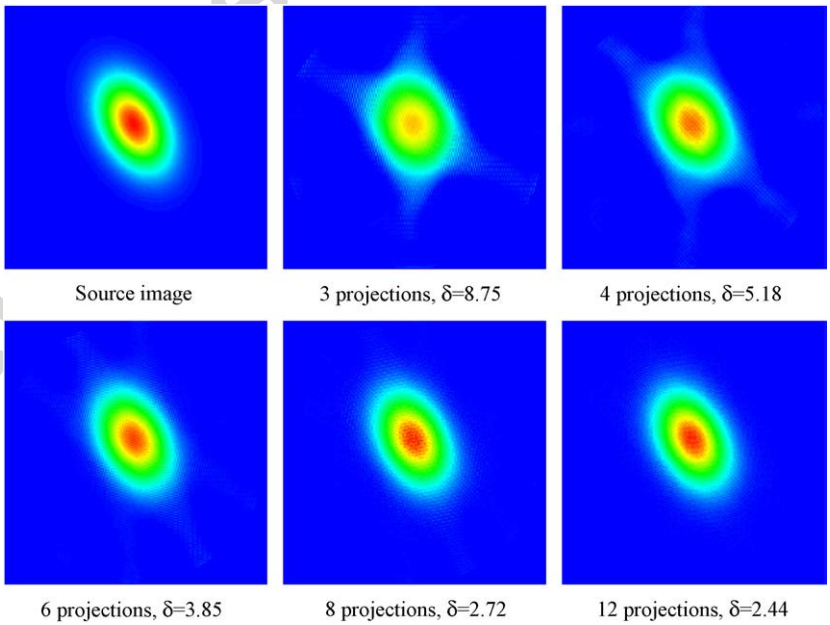

Fig. 3. Results of reconstruction of a strained Gaussian distribution.

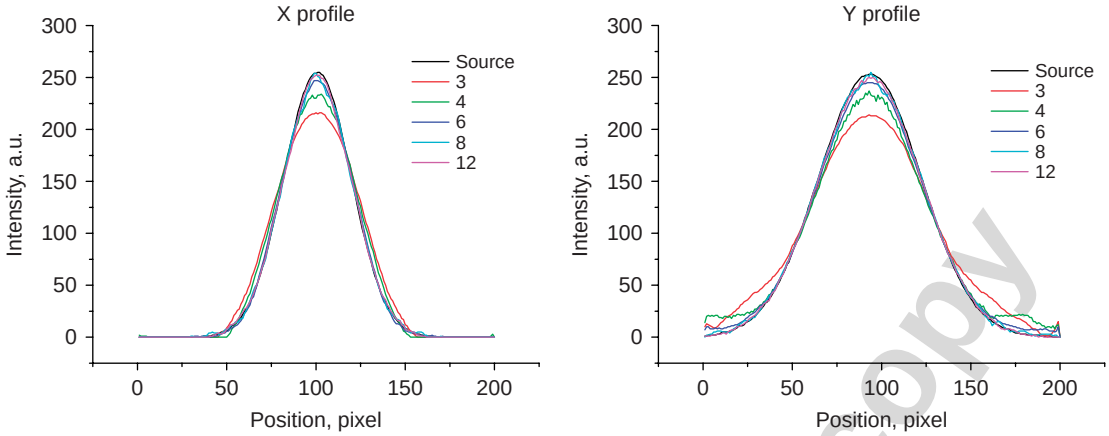

Fig. 4. X and Y profiles ($x_0 = 100$; $y_0 = 100$) of the source and reconstructed images vs the number of projections for the distribution presented in Fig. 3.

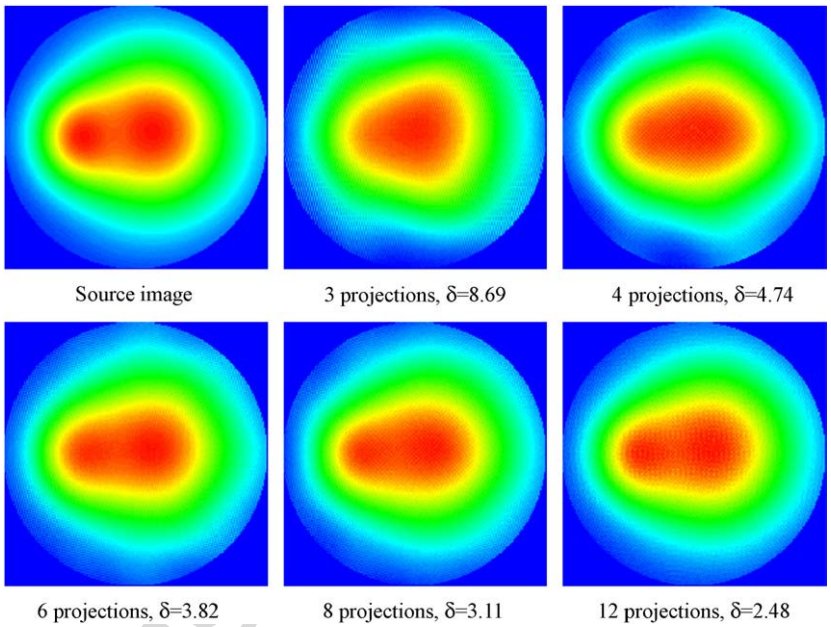

Fig. 5. Results of reconstruction of a synthetic image #1.

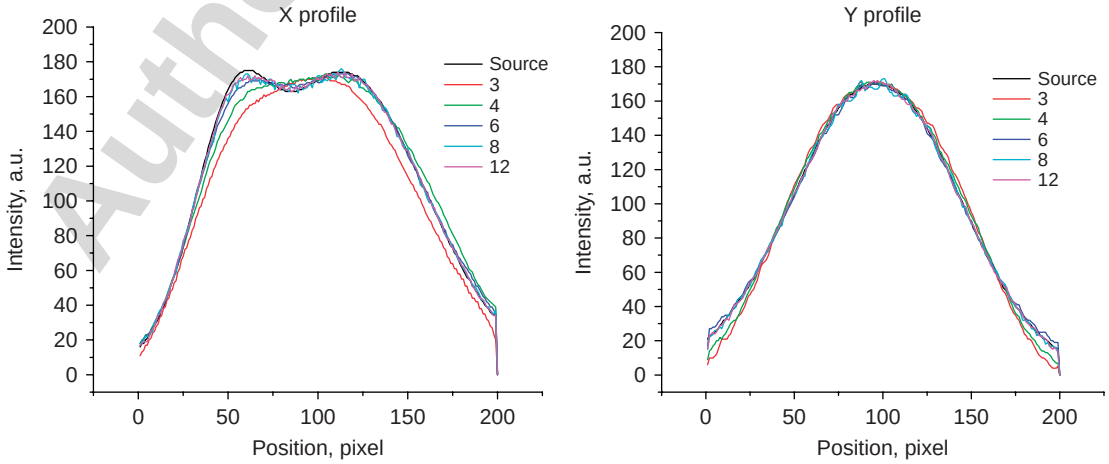

Fig. 6. X and Y profiles ($x_0 = 100$; $y_0 = 100$) of the synthetic image #1 vs the number of projections.

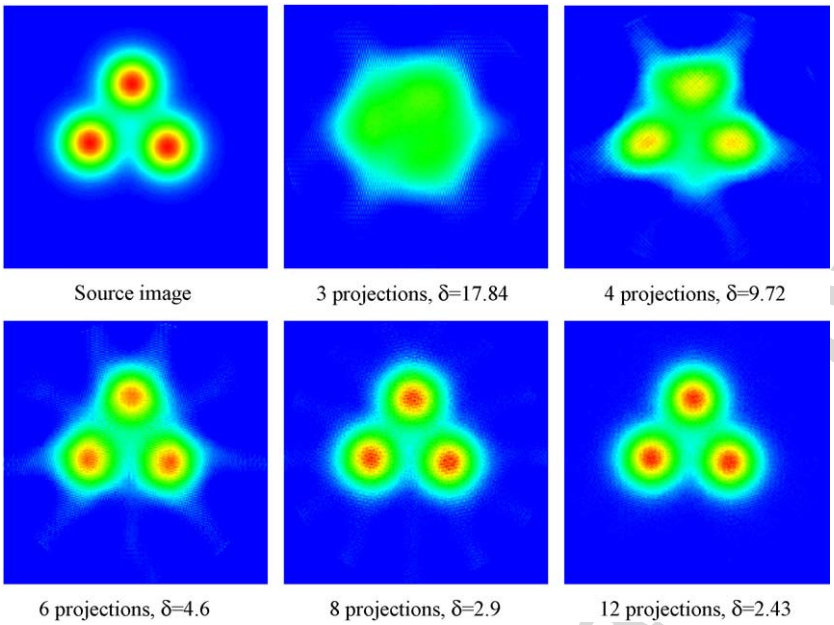

Fig. 7. Results of reconstruction of a synthetic image #2.

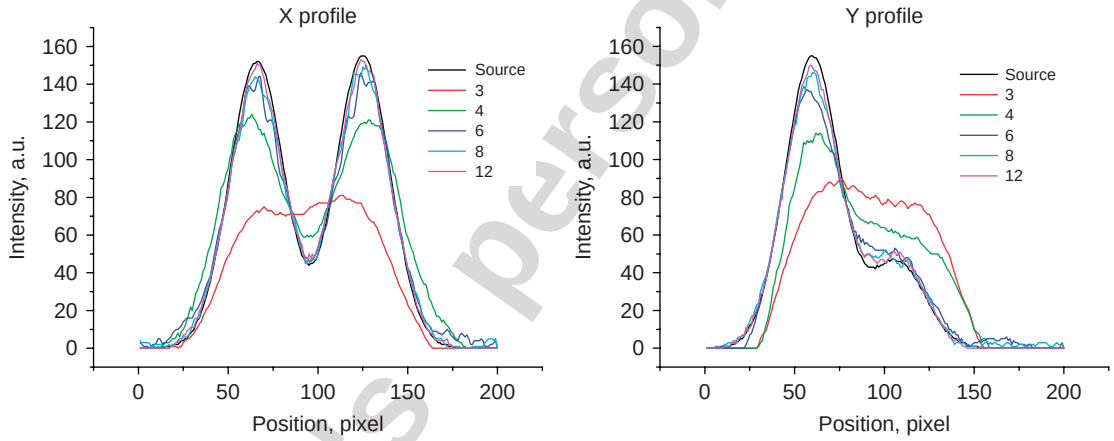

Fig. 8. X and Y profiles ($x_0 = 100$; $y_0 = 100$) of the synthetic image #2 vs the number of projections.

To make sure of the described algorithm efficiency when applied to an optical beam diagnostics, a numerical code IMPART has been developed. It performs mathematical processing of available projections using ART. The binary files containing real experimental data acquired with a CCD camera are used as input data. In addition, there is a possibility to simulate the data recording by drawing the necessary image projections from a test current density distribution defined by any bitmap grayscale graphic file.

Since the quality of the reconstruction depends not only on the number of used projections and points in each projection but also on the image itself, the first step consists to estimate the required number of projections in the test mode. Some test images of different structure were used as input data. The desired initial projections for subsequent reconstruction were calculated by numerical integration of the input images in the different directions. Usually, all the

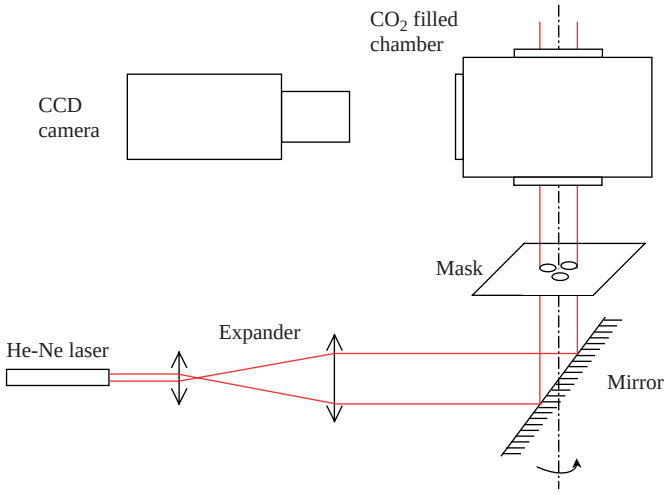

Fig. 9. Experimental setup.

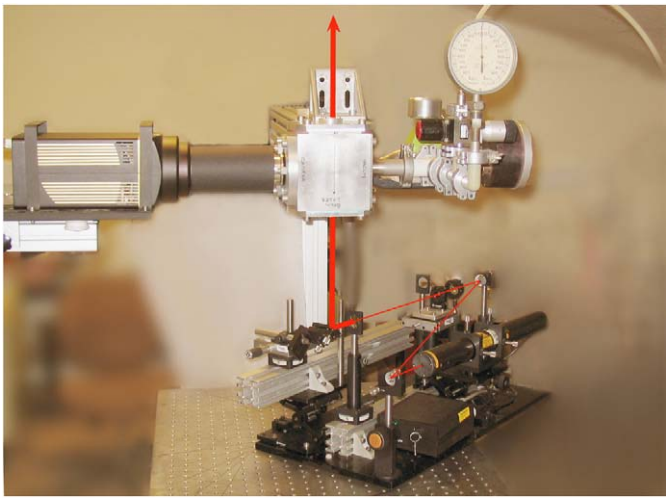

Fig. 10. View of the experimental workplace.

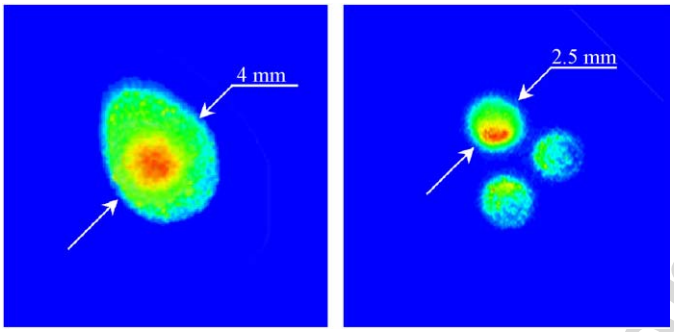

Fig. 11. The measured distributions of laser beam intensity in the cross-section: mask #1 (on the left) and mask #2 (on the right).

projection angles were distributed uniformly within the range $(0, \pi)$. The sets of three (30°, 90°, 120°), four (0°, 45°, 90°, 135°), six (0°, 30°, 60°, 90°, 120°, 150°), eight (0°, 22.5°, 45°, 67.5°, 90°, 112.5°, 135°, 157.5°), and twelve (0°, 15°, 30°, 45°, 60°, 75°, 90°, 105°, 120°, 135°, 150°, 165°) projections were used in the reconstruction. Each projection was composed of 200 points corresponding to the typical size of a CCD matrix.

The reconstruction quality is estimated using a conventional discrepancy indicator δ defined by the equation

$$\delta = \sqrt{\sum_{i,j}(e_{ij} - e'_{ij})^2 / N}$$

where e_{ij} and e'_{ij} are the original and reconstructed contents of the (i,j) pixel while N is the total number of pixels in each image. Being a quantitative measure, this indicator is not very illustrative. The discrepancy between the original image profiles and the reconstructed distributions seems to be a more obvious and comprehensive indicator. Therefore, in the figures presented below, in addition to the values of δ, two profiles $J(x) = j(x, y_0)$ and $J(y) = j(x_0, y)$ of the reconstructed images in both X and Y directions at $(x_0, y_0) = (100, 100)$ are plotted.

To make more pictorial the information about the reconstruction of images, they are converted and presented with multicolor scales as illustrated in Fig. 2.

According to the performed simulation, for the simple images (e.g., Fig. 3), the reconstructed profiles agree well with the original ones (with accuracy better than 20%) even if only three projections are used (Fig. 4). Six

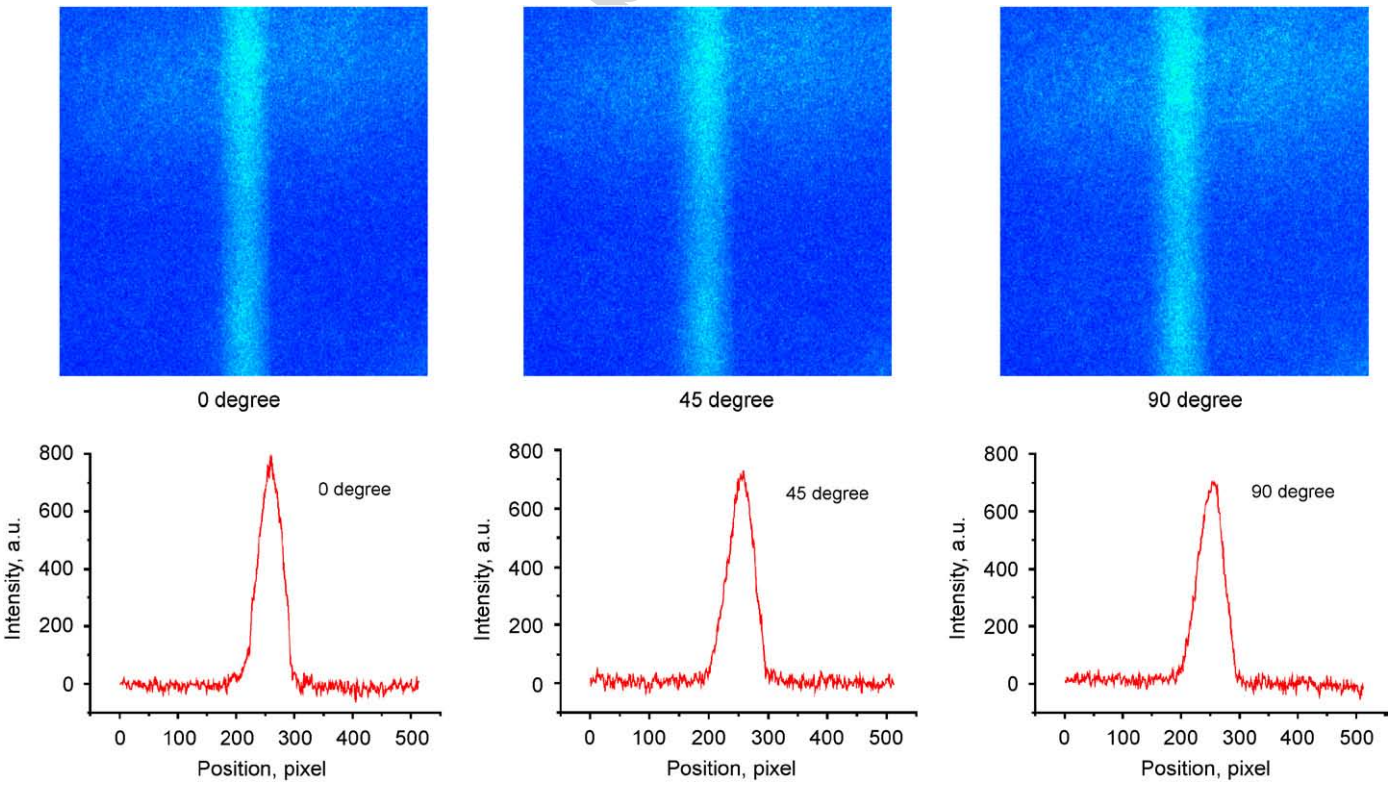

Fig. 12. Images recorded by the CCD camera and respective projections (mask #1).

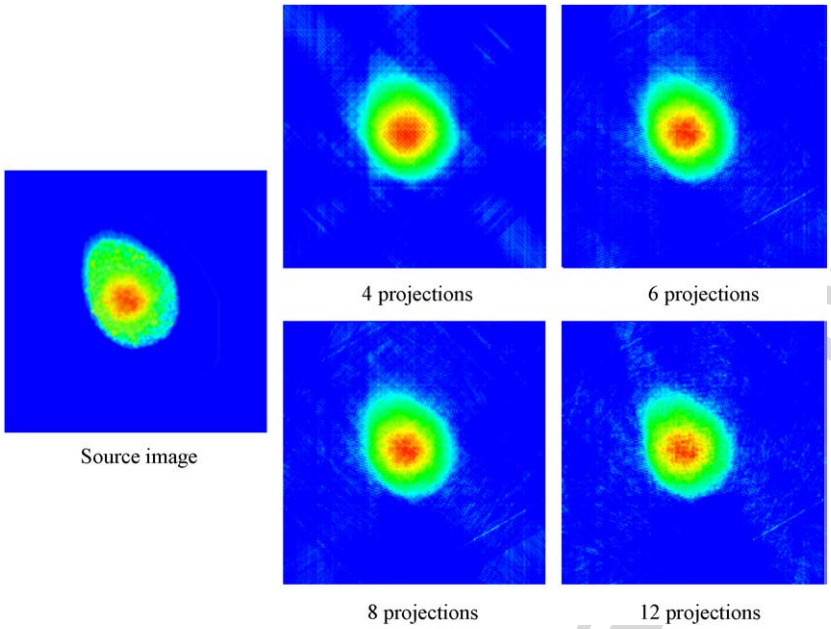

Fig. 13. The results of reconstruction of the image #1.

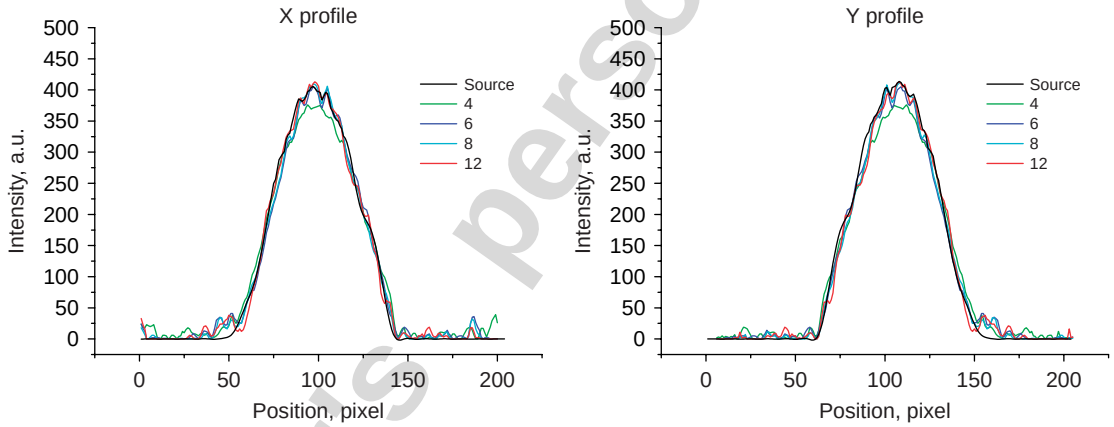

Fig. 14. X and Y profiles ($x_0 = 100$, $y_0 = 100$) of the source and reconstructed images vs the number of projections (mask #1).

projections provide a closer approximation in most cases (see e.g., Figs. 5 and 6). Only an accurate reconstruction of the most intricate images requires eight or even a greater number of projections (see e.g., Figs. 7 and 8).

3. Experimental results

To confirm the method efficiency, an experiment in conditions close to that of an ion beam has been carried out using the expanded beam of a He–Ne laser as object of a reconstruction. The experimental setup is presented schematically in Fig. 9.

The laser beam is expanded by two collecting lenses with different focal lengths up to a diameter of about 10 mm and directed into an experimental chamber filled with a fluorescent gas, through a first window. For the purpose, CO_2 at atmospheric pressure is used. The images are recorded by a CCD camera through another window. Instead of rotating the camera around the object, the object itself is revolved. The laser and optic system are placed on a rigid plate able to slide on a table around the chamber symmetry axis as shown in Fig. 10.

To better define the laser beam, some additional masks are placed along the beam line. The resulting intensity distributions in the beam cross-sections are recorded by substituting the gas filled chamber with a black screen rotated at 45° vs the beam axis. Because of an exposition duration, in this case, much shorter than for beam projections, the resulting picture is averaged up to a few of them.

The results of reconstruction of laser beam intensity distributions for two different masks (see Fig. 11) are

presented in Figs. 12–14 (mask #1) and Figs. 15–17 (mask #2).

Due to a weak light emission, the signal looks rather noisy. Nevertheless, a satisfactory agreement of the reference and reconstructed images is obtained.

4. Conclusion

The performed work demonstrates that, in most cases, 4–8 projections are sufficient to reconstruct the intensity distribution in the beam cross-section with a good

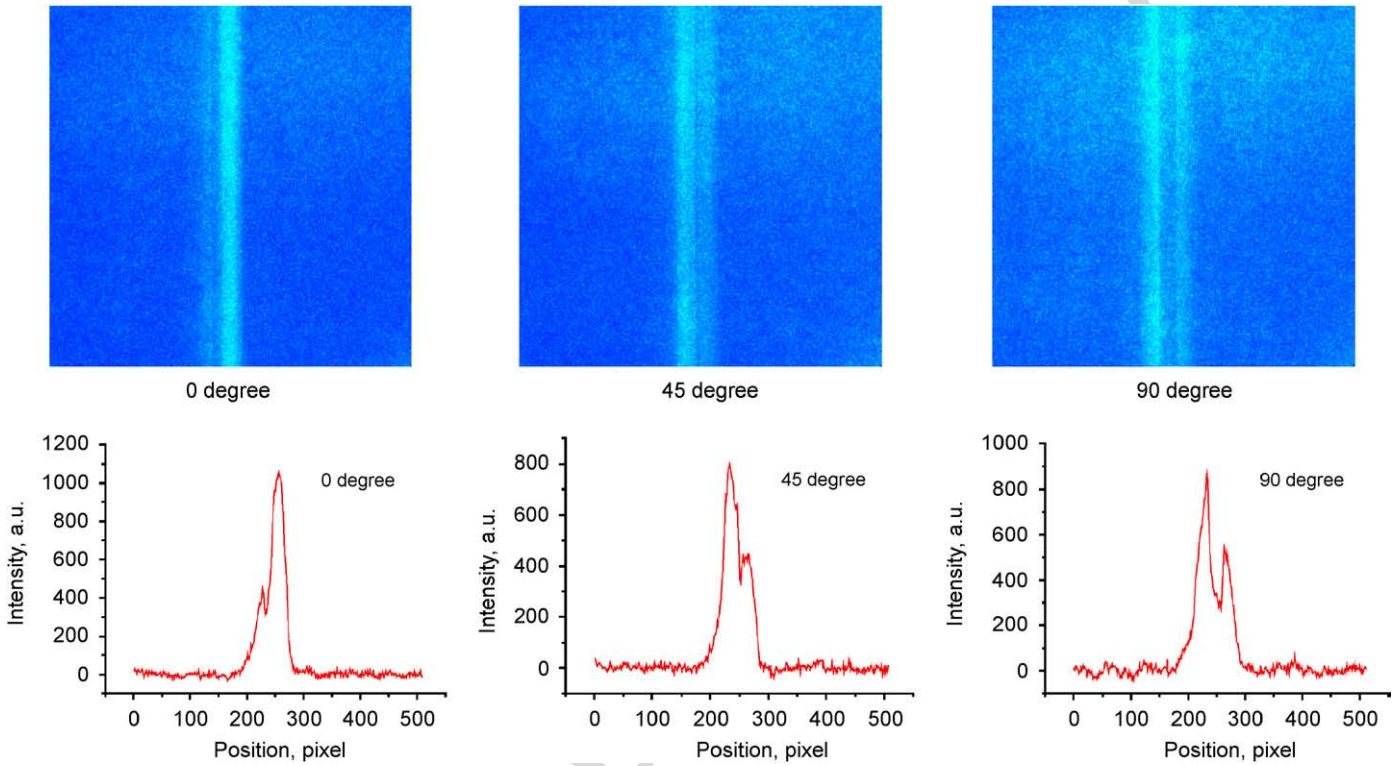

Fig. 15. Images recorded by CCD camera and respective projections (mask #2).

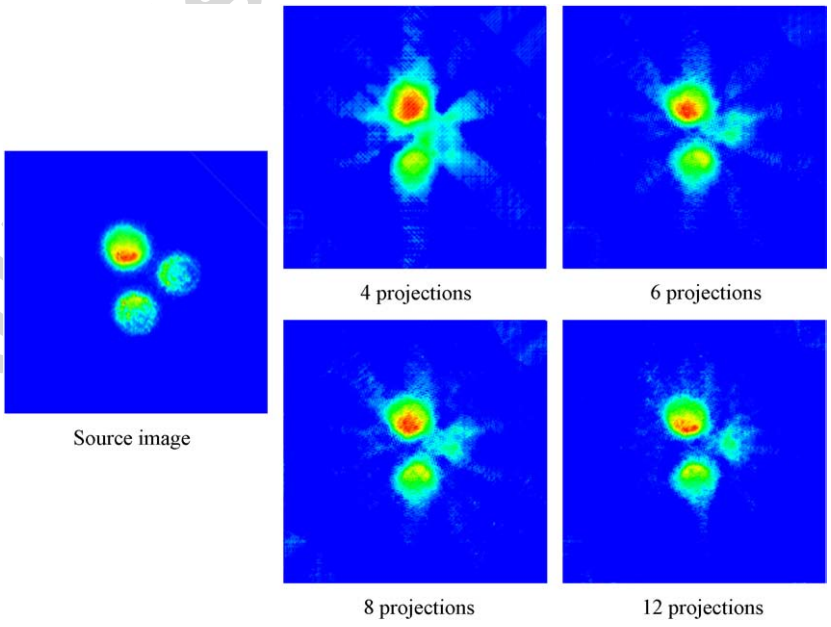

Fig. 16. The results of reconstruction of the image #2.

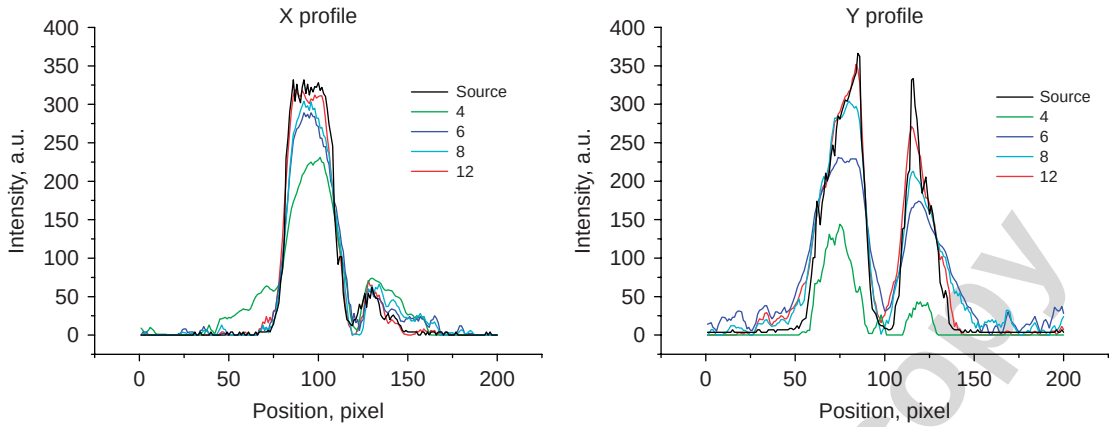

Fig. 17. X and Y profiles ($x_0 = 100$, $y_0 = 80$) of the source and reconstructed images vs the number of projections (mask #2).

accuracy. The next step would be to apply this diagnostics to ion beams. If the construction and manufacturing of a multi-window chamber presents few difficulties, the major remaining problem is the high cost of CCD cameras necessary to record all the projections simultaneously. The most reasonable way seems to be the development and application of an optical arrangement able to record all the projections with only one camera, since only a few rows of CCD matrix are commonly used to get each projection (10–20 from several hundreds available).

Acknowledgments

We are grateful to J.-P. Barbe for his help and valuable assistance during the experiments. We also would like to thank J. Arianer for careful reading of the manuscript.

References

[1] P. Ausset, S. Bousson, D. Gardès, et al., Optical transverse beam profile measurements for high power proton beams, EPAC-2002, Paris, June 2002.
[2] J. Radon, Ber. Verh. Sachs. Akad. Wiss. Leipzig, Math.-Phys. Kl 69 (1917) 262.
[3] R. Gordon, G.T. Herman, Int. Rev. Cytol. 38 (1974) 111.